Crystal chemistry and low-temperature properties of $Yb_{18}Pt_{51.1}Si_{15.1}$ ($\approx YbPt_3Si$)

E. Bauer, R. Lackner, G. Hilscher, and H. Michor
Institute of Solid State Physics, Vienna University of Technology, A-1040 Wien, Austria

E.-W. Scheidt and W. Scherer
Chemische Physik und Materialwissenschaften, Universität Augsburg, D-86159 Augsburg, Germany

P. Rogl
Institute of Physical Chemistry, University of Vienna, Währingerstrasse 42, A-1090 Wien, Austria

A. Gribanov, A. Tursina, and Y. Seropegin
Department of Chemistry, Moscow State University, 11992 Moscow, Russia

G. Giester
Institute of Mineralogy and Crystallography, University of Vienna, Althanstrasse 14, A-1090 Wien, Austria
(Received 8 August 2005; revised manuscript received 21 November 2005; published 8 March 2006)

$Yb_{18}Pt_{51.1}Si_{15.1}$ ($\approx YbPt_3Si$) is a representative in the series of $RPt_{\approx 3}Si$ compounds. The crystal structure of $Yb_{18}Pt_{51.1}Si_{15.1}$ has been determined from room temperature x-ray single crystal charge coupled device data: with $a=1.86246(3)$ nm; $c=0.40513(1)$ nm and space group $P4/mbm$. $Yb_{18}Pt_{51.1}Si_{15.1}$ is isotypic with the structures of $(Y,Dy)_{18}Pt_{50+x}Si_{16-x}$ revealing a curvilinear arrangement of distorted $CePt_3Si$-type fragments around Yb-centered cube-octahedra of $Pt_{12}[Yb]$. Similar to the structures of $(Y,Dy)_{18}Pt_{50+x}Si_{16-x}$ misfit regions with strong distortions are encountered as a typical feature of heavy rare-earth compounds $RPt_{\approx 3}Si$. On cooling, $Yb_{18}Pt_{51.1}Si_{15.1}$ orders antiferromagnetically below 1.8 K, followed by a second magnetic phase transition at 500 mK. Physical properties arise from the mutual influence of Ruderman-Kittel-Kasuya-Yosida interaction, the Kondo effect and crystal electric field (CEF) splitting, with the first excited CEF doublet more than 100 K above the ground state. The magnetic field dependence of the low-temperature heat capacity gives rise to a large magnetocaloric effect around 2 K.

DOI: 10.1103/PhysRevB.73.104405 PACS number(s): 75.80.+q, 71.20.Lp, 71.27.+a, 72.15.Qm

I. INTRODUCTION

$CePt_3Si$ ($CePt_3B$ type, $P4mm$) as the first heavy-fermion superconductor without a center of symmetry[1] has provided a wide playground to elucidate the mechanism of a possibly magnetically mediated type of superconductivity.[2–4] The missing inversion symmetry, in fact, seems to cause a distinct mixing of spin-singlet and spin-triplet components of the superconducting condensate.[5] However, not only the superconducting properties but also normal state physics of ternary $CePt_3Si$ and of isotypic homologous compounds RPt_3Si (R=La,Pr,Nd,Sm,Gd) show a number of interesting features.[6] Long-range antiferromagnetic order was encountered for R=Nd, Sm, and Gd. $PrPt_3Si$, however, does not show any sign of magnetic order down to 400 mK due to a nonmagnetic crystal effect field (CEF) ground state arising for the non-Kramers Pr^{3+} ion in tetragonal symmetry. A mean-field type of order is revealed for the spin-only case $GdPt_3Si$. CEF effects were conceived to be responsible for the observed deviation of T_N from a deGennes scaling. $TmPt_3Si$—although crystallizing in a derivative structure type—reveals a negative temperature coefficient of the electrical resistivity below room temperature.

Yb containing compounds in many cases exhibit anomalous physical properties at low temperature, similar to Ce systems. This fact is simply attributed to the mirrorlike electronic configuration of Ce and Yb systems. In a preponderant number of isomorphous compounds the valence state of cerium and ytterbium ions behaves such that the magnetic Ce^{3+} state corresponds in general to the nonmagnetic Yb^{2+} state. Superconductivity, however, has never been encountered in heavy-fermion-based Yb systems. The present work therefore intends to evaluate structure and physical properties of ternary $YbPt_3Si$ at low temperatures, in order to expand the knowledge of RPt_3Si compounds.

II. EXPERIMENTAL

Starting materials used were Y, Yb, and Pt ingots, 99.9 mass% pure, and Si pieces, 99.9999% which were argon arc melted in proper amounts on a water cooled copper hearth. Yb-vapor losses were compensated, and in combination with electron microprobe analyses (EMPA) a single phase composition was achieved via slight corrections of the Pt/Si content. The arc melted buttons were wrapped in Ta foil and vacuum sealed within thick-walled quartz tubes, heat treated at 800 °C for 10 days and quenched in water. X-ray examination and subsequent measurements of the various bulk properties on single phase polycrystalline materials were carried out with a series of standard techniques; details are given, e.g., in Ref. 7.

III. RESULTS AND DISCUSSION

A. Crystal chemistry of $Yb_{18}Pt_{51.1}Si_{15.1}$ ($YbPt_{\approx 3}Si$)

The x-ray powder pattern of $YbPt_3Si$ shows close resemblance to the intensity data recorded for the heavy rare-earth members with composition $RPt_{\approx 3}Si$. However, within the series of rare-earth containing compounds $RPt_{\approx 3}Si$ a variety of crystal structures has been hitherto discovered: whilst the light rare-earth members R=La, Ce, Pr, Nd, Sm, and Gd are all isotypic[6] with the noncentrosymmetric $CePt_3B$-type structure (space group $P4mm$), the heavier rare-earth elements seem to form structure variants with larger unit cells and centrosymmetry as encountered for $(Y,Dy)_{18}Pt_{50+x}Si_{16-x}$ [$(Y,Dy)_{18}Pt_{50+x}Si_{16-x}$-type, x=0.56 and 0.28, respectively; space group $P4/mbm$ (Ref. 8)] and $Er_{36}Pt_{102-x}Si_{32}$ with a closely related structure type [x=2.6; space group $P4_2/mnm$ (Ref. 9)]. As these structure types are difficult to differentiate from x-ray powder data, we intended to study the crystal structure of $YbPt_{\approx 3}Si$ on a suitable single crystal, obtained by mechanical fragmentation of an alloy with nominal composition $YbPt_3Si$, which was melted (at 1400 °C) under vacuum in a BN crucible and slowly cooled to 800 °C.

Inspection of selected crystals on an AXS-GADDS texture goniometer assured high crystal quality, unit cell dimensions and Laue symmetry of the specimens prior to x-ray intensity data collection on a four-circle Nonius Kappa diffractometer equipped with a CCD area detector employing graphite monochromated Mo$K\alpha$ radiation (λ =0.071073 nm). Orientation matrix and unit cell parameters for a tetragonal system were derived using the program DENZO.[10] No special absorption corrections were necessary because of the rather regular crystal shape and small dimensions of the investigated specimens. The structure was determined and refined with aid of the SHELXS-97 and SHELXL-97 programs.[11]

Systematic extinctions ($0kl$) for $k=2n+1$ and ($h00$) for $h=2n+1$ are compatible with several tetragonal space group types, of which $P4/mbm$ is the highest symmetric one. Employing direct methods determination of the atom arrangement was successful in the centrosymmetric space group $P4/mbm$, revealing a curvilinear arrangement of distorted $YbPt_3Si$ fragments ($CePt_3B$ type) around centered cube-octahedra Pt_{12}[Yb] at the origin and center of the unit cell. Similar to the structure type of $(Y,Dy)_{18}Pt_{50+x}Si_{16-x}$,[8] regions of severely distorted atom arrangements are encountered. In order to search for maximal atom order in these regions, structure refinements were pursued in the lowest possible symmetry $P4$. Refining anisotropic thermal displacement factors in the final run yielded an R value as low as R_{F^2}=0.058. However, search for symmetry elements (program MISSYM) confirmed $P4/mbm$ as the proper symmetry. Results of the final structure determination in $P4/mbm$ yield a structural formula of $Yb_{18}Pt_{51.1}Si_{15.1}$ (in atom percent $=Yb_{21.4}Pt_{60.7}Si_{17.9}$ in close correspondence with the EMPA data $Yb_{21.8}Pt_{60.0}Si_{18.2}$ (R_{F^2}=0.045)). Details of the structure determination (atom sites, atomic thermal displacement factors, etc.) will be published in a forthcoming paper.[12] The structure of $Yb_{18}Pt_{51.1}Si_{15.1}$ is presented in Fig. 1 in a three-dimensional view along the [001] axis. Platinum and silicon

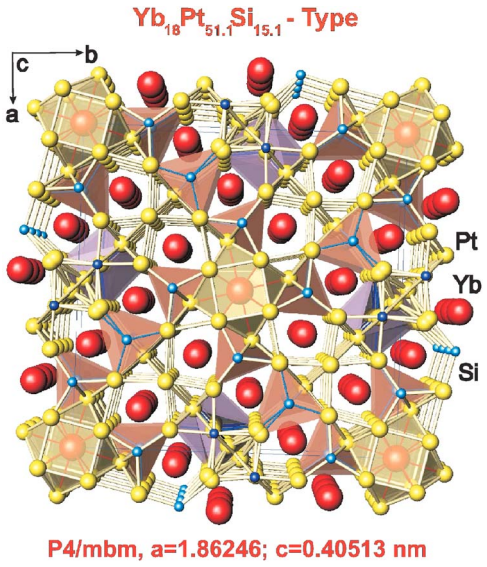

FIG. 1. (Color online) Crystal structure of $Yb_{18}Pt_{50}Si_{16}$ in three-dimensional view along the c axis.

atoms form a complex three-dimensional [$Pt_{51}Si_{15}$] network in which the crystallographically independent Yb atoms Yb1, Yb2, and Yb3, are located in three types of channels (distorted hexagonal, pentagonal, and tetragonal channels) running parallel to the c axis.

Coordination polyhedra for the three ytterbium sites are seen from Fig. 1. Whereas Yb1 and Yb2 atoms are at the centers of rather distorted polyhedra, Yb3 atoms are coordinated by a fairly symmetric cuboctahedron of 12 platinum atoms with interatomic Yb-Pt distances ranging from 0.2866 to 0.2887 nm. Yb1 atoms are coordinated by distorted hexagonal prisms with six additional atoms capping the rectangular faces [$Yb_2Pt_{10}Si_6$], CN=18. Yb2 atoms are at the center of distorted pentagonal prisms with centered rectangular faces [$Yb_1Pt_{12}Si_2$], CN=15.

Although the unit cell dimensions of $Yb_{18}Pt_{51.1}Si_{15.1}$ are much larger compared to the parent phase $CePt_3Si$, Fig. 1 reveals a close relationship. Centred around the fourfold axes, distorted $YbPt_3Si$ units of $CePt_3B$ type are the essential building blocks enclosing regions of severe structural distortions around the $2d$ site $(0,\frac{1}{2},0)$ (split atom positions for several Pt atoms, Pt/Si-random distribution in one site, atom dislocations from the higher symmetry site $2d$) as a typical feature of the RPt_3Si structures with the heavy-rare earth elements. Interatomic distances yield similar features also observed in $(Y,Dy)_{18}Pt_{50+x}Si_{16-x}$. Platinum-silicon distances range from 0.2272 to 0.2978 nm reflecting the distorted coordination figures. Shortest Yb-Yb distances are $d_{Yb1\text{-}Yb1}$ =0.3661 nm, followed by $d_{Yb1\text{-}Yb2}$=0.3810 nm, and $d_{Yb3\text{-}Yb3}$=0.4051 nm. Except for minor differences in the distorted regions, the structure of $Yb_{18}Pt_{51.1}Si_{15.1}$ can thus be considered as isotypic with the structures of $(Y,Dy)_{18}Pt_{50+x}Si_{16-x}$.[8]

The crystallographically derived chemical composition of the new compound finally served to successfully synthesize single-phase bulk material thereby confirming the results of the structural investigation. The minor deviation from the

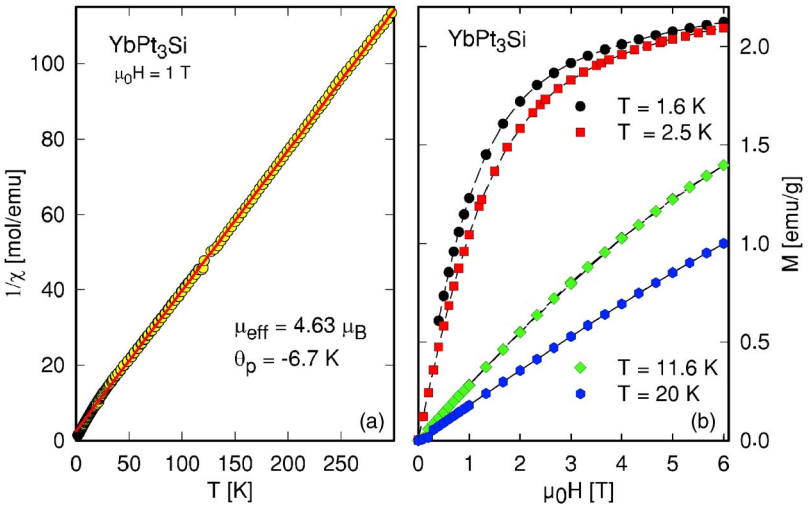

FIG. 2. (Color online) (a) Temperature-dependent magnetic susceptibility χ of $YbPt_3Si$ plotted as $1/\chi$ vs T. The solid line is a least squares fit according to the modified CW law. (b) Isothermal magnetization M vs $\mu_0 H$ of $YbPt_3Si$.

ideal stoichiometry $YbPt_3Si$ lies within 1.5 atom percent and thus may justify the fact that in the following we will simply address the new compound as $YbPt_3Si$.

B. Bulk properties

In order to characterize physical behavior of the ternary rare-earth compound $YbPt_3Si$, temperature-dependent magnetic, thermodynamic, and transport properties were studied. To define the phonon contributions to the total measured effects, the corresponding quantities have also been investigated for isostructural, nonmagnetic YPt_3Si.

Figure 2(a) shows the temperature-dependent magnetic susceptibility χ plotted as χ^{-1} vs T for $YbPt_3Si$ from 2 to 300 K. Above about 50 K a Curie-Weiss-like behavior indicates a simple paramagnetic state. To quantatively account for this region, a least squares fit according to the modified Curie Weiss law, i.e., $\chi=\chi_0+C/(T-\theta_p)$ was applied. $\chi_0=2.5\times10^{-7}$ emu/mol represents a temperature-independent Pauli-like susceptibility, C is the Curie constant yielding an effective moment $\mu_{\text{eff}}=4.63\mu_B$ and $\theta_p=-6.7$ K is the paramagnetic Curie temperature. The effective magnetic moment is close to the theoretical value associated with the Yb^{3+} state. The slight curvature of the inverse magnetic susceptibility observed below 50 K is attributed to crystal electric field (CEF) effects.

Isothermal magnetization M vs $\mu_0 H$ of $YbPt_3Si$ for various temperatures, as displayed in Fig. 2(b), appears to be strongly curved at low temperatures and approaches saturation with $M\approx2.1\mu_B$/Yb at $\mu_0 H=6$ T. CEF effects as inferred from the susceptibility data $\chi(T)$ are expected to be responsible for the significant deviation from the ideal saturation moment of $M(Yb^{3+})=4\mu_B$. No spontaneous magnetisation has been revealed from Arrott plots, indicating the absence of ferromagnetic order down to 1.6 K.

Long-range magnetic order, however, is clearly evidenced from heat capacity data as plotted in the inset of Fig 3. Down to about 50 mK, $YbPt_3Si$ exhibits two magnetic phase transitions at $T_{m1}\approx1.8$ K and at $T_{m2}\approx0.5$ K. While the phase transition at T_{m1} appears to be quite sharp and narrow, the one at T_{m2} seems to be much broader. As a consequence, $C_p(T)$ becomes only weakly temperature dependent for $T_{m2}<T<T_{m1}$, thus containing a significant amount of entropy. Two possibilities are conceivable to explain these transitions. (i) A presumably antiferromagnetic ordered state, which sets in around 1.8 K, undergoes a second phase transition at $T_{m2}\approx0.5$ K. (ii) Since the crystallographic unit cell of $YbPt_3Si$ possesses three fully occupied inequivalent lattice sites for the Yb ions (Yb at $8i_1$, $8i_2$, $2a$), magnetic order even with different magnetic structures and ordering temperatures may be enabled on the respective Yb sublattices. The scenario sketched has yet to be proven by elastic neutron-scattering experiments. The effective magnetic moment, found to be very close to the theoretical value of Yb^{3+}, obviously indicates that the electronic configuration of the Yb ions on *each* lattice site is very near to the magnetic $4f^{13}$ state.

The specific heat of $YbPt_3Si$ is plotted over an extended temperature range in Fig. 3 as C_p/T vs T. In order to properly define the magnetic contribution to the specific heat,

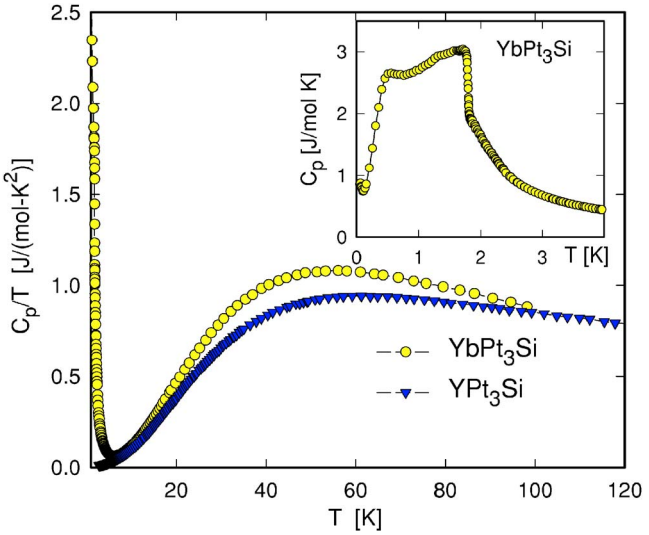

FIG. 3. (Color online) Temperature-dependent specific heat C_p of $YbPt_3Si$ and YPt_3Si plotted as C_p/T vs T. The inset shows low-temperature specific-heat features of $YbPt_3Si$.

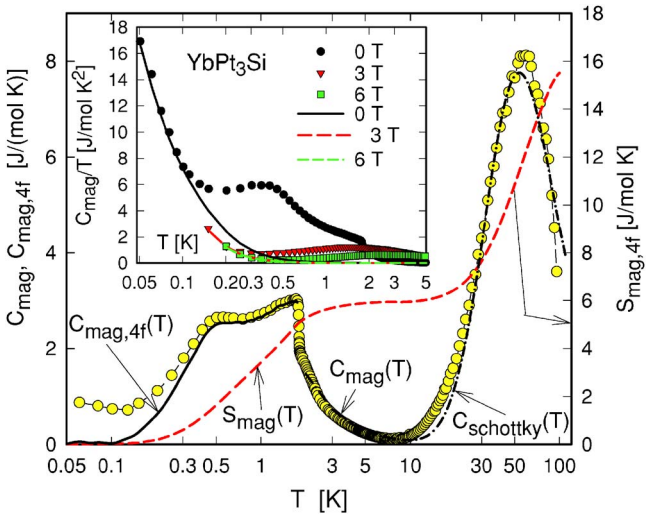

FIG. 4. (Color online) Magnetic contribution to the specific heat $C_{\mathrm{mag}}(T)$ (filled circles) and $C_{\mathrm{mag},4f}(T)$ (solid line) of $YbPt_3Si$. The dashed-dotted line is a fit of a Schottky anomaly with excited doublets at 110, 170, and 190 K, respectively. The dashed line represents the magnetic entropy $S_{\mathrm{mag},4f}$ (right axis). The inset shows the low temperature dependence of C_{mag} plotted as C_{mag}/T vs T for 0, 3, and 6 T. The solid and the dashed lines are fits of the core contribution C_{nuc}.

measurements of $C_p(T)$ have been performed for the homologue YPt_3Si. Nonmagnetic $LuPt_3Si$ has not yet been observed in the $P4/mbm$-type crystal structure. YPt_3Si exhibits a smooth temperature dependence of $C_p(T)$ and a standard analysis of the low-temperature data yields $\gamma = 2.5\ \mathrm{mJ/mol\,K^2}$, and $\theta_D^{\mathrm{LT}} = 217$ K. A Sommerfeld value of $2.5\ \mathrm{mJ/mol\,K^2}$ is quite reasonable for simple metallic systems without substantial electron correlations and without a strong enhancement due to electron-phonon interaction. Here, it is interesting to note that nonmagnetic $LaPt_3Si$ is characterized by a much larger density of states at the Fermi energy as evidenced by a Sommerfeld value of about $9\ \mathrm{mJ/mol\,K^2}$[21].

Employing the Debye function to quantitatively describe the overall temperature dependence of $C_p(T)$ of YPt_3Si does not work convincingly, except in a narrow temperature region at low temperatures, yielding essentially the above indicated parameters. In general, deviations from the simple Debye function are referred to the presence of Einstein-like contributions to the phonon spectrum. A plot of C_p/T^3 vs T of YPt_3Si yields a local maximum around $T = 14$ K, corresponding to Einstein modes with significant spectral weight around $\theta_E \approx 70$ K. Certainly, from the very complex structure of both YPt_3Si and $YbPt_3Si$ one expects a broad spectrum of additional Einstein frequencies.

A comparison of the heat capacities of $YbPt_3Si$ and YPt_3Si in Fig. 3 allows us to determine the magnetic contribution to the specific heat C_{mag}. Since data for $YbPt_3Si$ are taken down to about 50 mK, a significant core contribution C_{nuc} is added up to the raw data roughly below 500 mK (compare inset, Fig. 4). In order to derive $C_{\mathrm{nuc}}(T)$ from the present measurement a nuclear Schottky term has been calculated taking into account an externally applied magnetic field B_{ext}, an effective (hyperfine) magnetic field arising from orbital and conduction electrons B_{int} and in noncubic crystals, an electric field gradient V_{zz}. We have calculated the hyperfine contributions to the heat capacity originating from the quadrupole moment of ^{173}Yb and from the nuclear magnetic moments of ^{29}Si, ^{173}Yb, and ^{195}Pt. The fits are shown as solid and dashed lines in the inset of Fig. 4, yielding for zero magnetic field $B_{\mathrm{int}} = 39$ T and $V_{zz} = 29 \times 10^{22}\ \mathrm{V/m^2}$. In an applied external magnetic field of $B_{\mathrm{ext}} = 3$ and 6 T the electric field gradient V_{zz} is reduced to 16.5 and $15.5 \times 10^{22}\ \mathrm{V/m^2}$, respectively, while B_{int} remains constant. The large field gradients are likely to be a consequence of weak disorder arising in the complex crystal structure. Taking into account $C_{\mathrm{nuc}}(T)$, the magnetic contribution $C_{\mathrm{mag},4f}(T)$ due to the Yb $4f$ electrons can be evaluated, i.e., $C_{\mathrm{mag},4f}(T) \approx C_p(YbPt_3Si) - C_{\mathrm{nuc}}(YbPt_3Si) - C_p(YPt_3Si)$, plotted in Fig. 4. Two distinct features can be recognized. (i) The low-temperature peaks correspond to magnetic ordering at $T_{m1} = 1.8$ K and $T_{m2} = 0.5$ K, respectively. (ii) Lifting the eightfold degenerate $(N = 2j+1)$ total angular momentum $j = 7/2$ by CEF effects in tetragonal symmetry causes a ground-state doublet and additionally three doublets at elevated energies. Within the mean-field model, the corresponding jump of the specific heat at the ordering temperature amounts to 12.5 J/mol K. As the actual value $\delta_C \approx 3$ J/mol K at $T = T_{m1}$ of $YbPt_3Si$ is well below an unperturbed doublet as ground state, an appropriate mechanism has to be involved. In addition to the second phase transition at T_{m2}, Kondo type interactions are known to significantly suppress the specific heat anomaly at $T = T_m$. A Kondo effect normally occurs in Ce- and Yb-based compounds and is obvious from resistivity measurements on $YbPt_3Si$ as well (see below).

Kondo type interactions cause, in theory,[13] a progressive diminuation of δ_C vs T_K/T_m, where T_K is the Kondo temperature of the system. Applying $T_m \approx 1.8$ K to this model reveals $T_K \approx 3.1$ K, a value reasonably placed with respect to the paramagnetic Curie temperature $\theta_p \approx -7$ K. θ_p of Kondo systems is frequently taken as a measure of the characteristic temperature of the system, i.e., $T_K \approx \theta_p/4$.[14] Further evidence for Kondo-type interaction with a small characteristic temperature follows from a roughly 15% reduction of the entropy at $T = T_{m1}$ in comparison to magnetic ordering within a simple CEF doublet as ground state.[15]

Elucidating the $S_{\mathrm{mag},4f}$ vs T dependency provides additional arguments for a doublet as a ground state. (i) The low-temperature entropy release exhibits a plateaulike region with values near to $R \ln 2$ [$S_{\mathrm{mag},4f}(10\ \mathrm{K}) = 5.95$ J/mol K]. (ii) Further release of entropy corresponds to the maximum in $C_{\mathrm{mag}}(T)$, representing a Schottky anomaly. (iii) The presence of a plateau in $S_{\mathrm{mag},4f}(T)$ below about 10 K strongly hints at excited CEF levels which are well separated from the ground state doublet. The position of the maximum in $C_{\mathrm{mag}}(T)$ indicates that the first excited CEF level is unlikely to be situated below 100 K.

In a more quantitative manner, the splitting of the $j = 7/2$ total angular momentum by the CEF in tetragonal symmetry can be illustrated involving a ground state doublet and three excited levels in terms of a Schottky contribution. This contribution to the specific heat is caused by the thermal

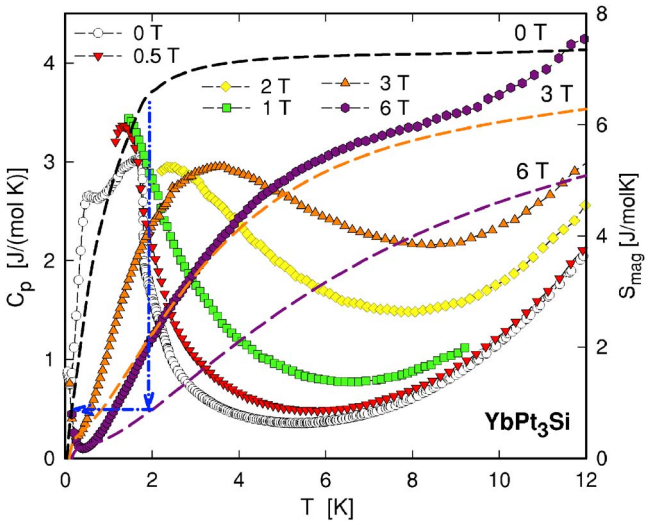

FIG. 5. (Color online) Magnetic field dependence of the specific heat $C_p(T)$ of $YbPt_3Si$. The dashed lines represent the temperature-dependent magnetic entropy $S_{mag}(T)$ at $\mu_0 H=0$, 3, and 6 T (right axis), including the core contribution as well. The dashed-dotted lines sketch a cooling stage at $T=2$ K.

population of the various crystal field levels and the thus resulting increase of the free energy F of the system:

$$F = \frac{R\sum_{r=0}^{m} \Delta_r g_r \exp\left(\frac{-\Delta_r}{k_B T}\right)}{\sum_{r=0}^{m} g_r \exp\left(\frac{-\Delta_r}{k_B T}\right)}. \quad (1)$$

g_r is the degeneracy of the rth level, Δ_r the energy difference to the ground state, and R the gas constant ($R=8.314$ J/mol K). In a first approximation we have adopted an averaged CEF for the three crystallographically inequivalent Yb sites. Equation (1) allows a calculation of the Schottky contribution to the specific heat. Thereby, the ground-state (g.s.) doublet is assumed to be split by long-range magnetic order and/or the Kondo effect with an effective interaction strength of 3 K. The first, second, and third excited levels are situated at 110, 170, and 190 K above the ground state, respectively. The result of this procedure is shown as a dashed-dotted line in Fig. 4, yielding fair agreement with the experimental data and confirms the conclusions drawn above. A slight variation of both uppermost CEF levels is, of course, insignificant with respect to the experimental data measured up to 100 K.

The field dependence of the specific heat was studied in external fields of 3 and 6 T down to 0.1 K and for various other fields down to 1.15 K (Fig. 5). The field dependence reveals, initially at 0.5 T, a smearing of the anomaly at 1.8 K without any significant shift in temperature. For fields $\mu_0 H \geqslant 1$ T a transformation to a Zeeman-type Schottky anomaly is observed together with a small low-temperature contribution due to residual magnetic correlations.

The magnetic entropy S_{mag} for the 0, 3, and 6 T data is derived from the respective heat capacity by subtracting $C_p(YPt_3Si,T)$, and finally integrating $C_{mag}/T(T,\mu_0 H)$. With respect to the 0 T data, the entropy gain at 3 and 6 T is substantially reduced, particularly in the low-temperature limit. The fact that in the zero T case the entropy gain at temperatures below 1 K [$S_{mag}(1\text{ K}) \simeq 4.2$ J/mol K] which can be easily spread to higher temperatures by relatively small fields of a few T, makes $YbPt_3Si$ suitable for magnetocaloric applications in the He temperature range. A quantitative estimation of the magnetocaloric effect shows that an isothermal increase of the magnetic field from zero to 6 T at, e.g., $T=2$ K and the subsequent removal of the magnetic field results in a temperature decrease to well below 0.4 K (dashed-dotted line). In particular, the large heat capacity of about 2 J/mol K at 300 mK supports the usability of $YbPt_3Si$ as magnetocaloric material.

The temperature-dependent electrical resistivity $\rho(T)$ of $YbPt_3Si$ and YPt_3Si is plotted in Fig. 6(a) from 600 mK to room temperature. Overall resistivity values are rather large in comparison to equally prepared light rare earth RPt_3Si with the $CePt_3B$-type structure.[6] As an example, the room-temperature resistivity values for R=La,Ce are 57.3, 88.3 $\mu\Omega$ cm, respectively, while those of Y and Yb samples are 182 and 189 $\mu\Omega$ cm. This distinct difference may be a consequence of the more complex crystal structure of both latter compounds, giving rise to enhanced scattering pro-

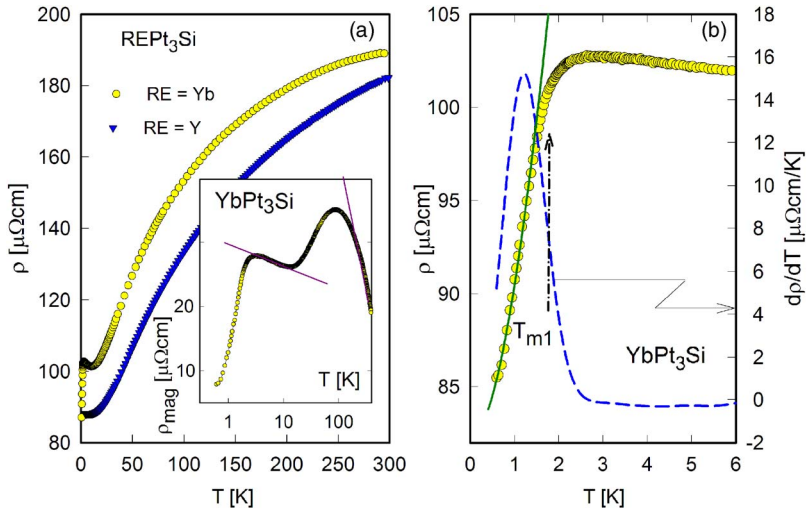

FIG. 6. (Color online) (a) Temperature-dependent resistivity ρ of $YbPt_3Si$. The inset displays $\rho_{mag}(T)$ vs $\ln T$. (b) Low-temperature resistivity of $YbPt_3Si$. The dashed line represents the derivative $d\rho/dT$ and the solid line is a least squares fit according to Eq. (2).

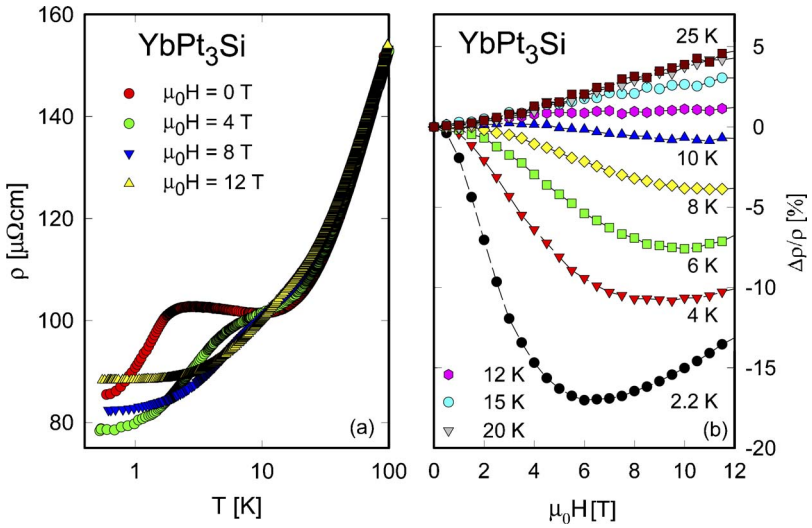

FIG. 7. (Color online) (a) Temperature-dependent resistivity ρ of $YbPt_3Si$ for various values of applied magnetic fields. (b) Isothermal magnetoresistance $\Delta\rho/\rho$ of $YbPt_3Si$ for various temperatures.

cesses of the conduction electrons on static lattice imperfections.

While YPt_3Si shows metallic behavior, $YbPt_3Si$ displays anomalous features due to the onset of long-range magnetic order below 1.8 K, due to the Kondo effect as well as due to CEF splitting. Similar to the specific heat, however, a standard model such as the Bloch Grüneisen formula, describing the interactions of electrons with thermally excited phonons, is insufficient to account for $\rho(T)$ of YPt_3Si. Even adding a Mott-Jones like term, i.e., κT^3, does not allow a convincing least squares fit.

The influence of charge carrier scattering on the magnetic moments of Yb is revealed in detail after subtracting the phonon contribution ρ_{ph} from the total measured effect, where $\rho_{ph}(T)$ is approximated by $\rho(T)$ of isomorphous YPt_3Si. Resulting $\rho_{\mathrm{mag}}(T)$ of $YbPt_3Si$ is displayed in the inset of Fig. 6(a) on a logarithmic temperature scale. The overall features of $\rho_{\mathrm{mag}}(T)$ constitute a textbook-like example of a Kondo lattice system in presence of strong CEF splitting, and long-range magnetic order at low temperatures. The logarithmic regime of $\rho_{\mathrm{mag}}(T)$ at lower temperatures represents the Kondo effect in the CEF ground state, whereas the logarithmic dependency at higher temperatures reflects Kondo-type scattering in the total angular momentum state $j=7/2$. This distinct behavior closely obeys the theoretical model of Cornut and Coqblin,[16] derived from the Anderson Hamiltonian in terms of perturbation-type calculations. The significant drop below 2 K clearly manifests the onset of long-range magnetic order, reducing magnetic scattering processes.

A superzone boundary effect as the cause of the negative temperature coefficient of $\rho(T)$ above T_{m1}—forming an additional Brillouin zone[17]—is rather unlikely, because the monotonous decrease of $\rho(T)$ extends over a temperature region of about 10 K (around 5 times the ordering temperature).

Further details of the low-temperature resistivity of $YbPt_3Si$, particularly in the magnetically ordered state are plotted in Fig. 6(b). The magnetic transition temperature T_{m1} was observed from the temperature derivative $d\rho/dT$ (dashed line, right axis). Taking the inflection point of $d\rho/dT$ as the ordering temperature reveals $T_{m1}=1.75$ K.

In an attempt to describe the magnetically ordered region in the $\rho(T)$ plot of $YbPt_3Si$, a model developed in Ref. 18 is applied, yielding an analytic expression concerning the temperature- dependent electrical resistivity

$$\rho = \rho_0 + A\Delta^{3/2}T^{1/2}\exp(-\Delta/T)\left[1+\frac{2}{3}\left(\frac{T}{\Delta}\right)+\frac{2}{15}\left(\frac{T}{\Delta}\right)^2\right]. \tag{2}$$

This expression is based on scattering of conduction electrons on antiferromagnetic magnons with a dispersion relation given by $\omega=\sqrt{\Delta^2+D^2k^2}$, where Δ is the spin-wave gap and D is the spin-wave velocity; $A\propto 1/D^3\propto 1/\Gamma^3$ and Γ is an effective magnetic coupling among Yb ions. Applying Eq. (2) to the experimental data yields a gap $\Delta\approx 1$ K, $\rho_0=83$ $\mu\Omega$ cm, and $A=11$ $\mu\Omega$ cm K^{-2}. Despite the data set is limited to the narrow temperature range between the two magnetic phase transitions ($0.5<T<1.8$ K), the spin-wave gap obtained is of reasonable order with respect to the magnitude of the ordering temperature.

The temperature-dependent electrical resistivity for various values of external magnetic fields up to 12 T is displayed in Fig. 7(a). Magnetic order appears to be suppressed by magnetic fields above about 8 T as the most prominent feature of the magnetoresistance measurement. Analyzing the 8 T run according to $\rho=\rho_0+AT^n$ reveals an exponent $n\approx 1.42$, in good agreement with a three-dimensional antiferromagnet near to the quantum critical point. For temperatures below 1 K, the resistivity firstly decreases with fields but above 4 T the trend is inverted yielding the highest resistivity value for a field of 12 T at about 0.8 K.

The magnetoresistance $\Delta\rho/\rho$ as a function of external magnetic fields for various temperatures from 2.2 to 25 K is shown in Fig. 7(b). In agreement with the trend described above, $\Delta\rho/\rho$ is negative for low temperatures, but above about 12 K becomes positive. The complex field and temperature behavior may be interpreted in terms of two major antagonistic influences, (i) the dominating Kondo effect (negative contribution) and (ii) the classical magnetoresistance of a metallic system (positive contribution). Moreover,

the measurement at 2.2 K comprises additional influences from short range order effects in the proximity of the magnetic transition.

IV. SUMMARY

$Yb_{18}Pt_{50}Si_{16}$ is a representative in the series of $RPt_{\approx 3}Si$ compounds isotypic with the structures of $(Y,Dy)_{18}Pt_{50+x}Si_{16-x}$. The crystal structure consists of $CePt_3B$-type building units with areas of strongly distorted regions in between.

Measurements of the magnetic susceptibility and isothermal magnetization, specific heat in external magnetic fields, and field-dependent resistivity measurements reveal a trivalent ground state for the Yb ion, giving rise to a stable $4f^{13}$ electronic configuration of the system. Long-range antiferromagnetic order sets in at $T=1.8$ K with a spin-wave gap of the order of 1 K. Below 0.5 K a further magnetically ordered state occurs. The paramagnetic temperature regime is characterized by the interaction of the Kondo effect and crystal electric field splitting. The tetragonal crystal structure causes a lifting of the eightfold degenerate $j=7/2$ total angular moment of the Yb ion, resulting in a manifold of four doublets with the first excited CEF level separated by more than 100 K from the ground state. Hence, magnetic order occurs within the ground-state doublet which, additionally, is evidenced from magnetic entropy data. The field dependence of the heat capacity supports an enormous magnetocaloric effect around 2 K, revealing a high potential to realize efficient sample cooling to temperatures well below 1 K.

ACKNOWLEDGMENTS

This research was sponsored by the Austrian FWF under grants Nos. P18054, P16370, and P16250. The authors are grateful to COST P16 "ECOM" and the OEAD for support within the framework of the Austrian-Russian bilateral exchange program within Project Nos. I.18/4, RFBR 03-03-20001BNTS-a, and RFBR 05-03-33045.

[1] E. Bauer, G. Hilscher, H. Michor, Ch. Paul, E.-W. Scheidt, A. Gribanov, Yu. Seropegin, H. Noel, M. Sigrist, and P. Rogl, Phys. Rev. Lett. **92**, 027003 (2004).

[2] M. Yogi, Y. Kitaoka, S. Hashimoto, T. Yasuda, R. Settai, T. D. Matsuda, Y. Haga, Y. Onuki, P. Rogl, and E. Bauer, Phys. Rev. Lett. **93**, 027003 (2004).

[3] K. V. Samokhin, E. S. Zijlstra, and S. K. Bose, Phys. Rev. B **69**, 094514 (2004).

[4] P. A. Frigeri, D. F. Agterberg, A. Koga, and M. Sigrist, Phys. Rev. Lett. **92**, 097001 (2004).

[5] D. Agterberg, Physica B (to be published).

[6] E. Bauer, R. Lackner, G. Hilscher, H. Michor, M. Sieberer, A. Eichler, A. Gribanov, Yu. Seropegin, and P. Rogl, J. Phys.: Condens. Matter **17**, 1877 (2005).

[7] E. Bauer, St. Berger, Ch. Paul, M. D. Mea, G. Hilscher, H. Michor, M. Reissner, W. Steiner, A. Grytsiv, P. Rogl, and E. W. Scheidt, Phys. Rev. B **66**, 214421 (2002).

[8] A. I. Tursina, A. V. Gribanov, H. Noel, P. Rogl, and Y. D. Seropegin, J. Alloys Compd. **1395**, 93 (2005).

[9] A. I. Tursina, A. Gribanov, H. Noel, P. Rogl, and Y. Seropegin, Acta Crystallogr. **60**, i8 (2004).

[10] Nonius Kappa CCD Program Package COLLECT, DENZO, SCALEPACK, SORTAV (Nonius Delft, 1998).

[11] G. M. Sheldrick, SHELXL-97, Program for Crystal Structure Refinement, University of Gttingen, Germany, 1997; Windows version by McArdle, National University of Ireland, Galway.

[12] P. Rogl (private communication).

[13] M. Besnus, A. Braghta, N. Hamdaoui, and A. J. Meyer, J. Magn. Magn. Mater. **104-107**, 1385 (1992).

[14] A. Hewson, *The Kondo Problem to Heavy Fermions* (Cambridge University Press, Cambridge, 1993).

[15] H. U. Desgranges and K. D. Schotte, Phys. Lett. **91**A, 240 (1982).

[16] D. Cornut and B. Coqblin, Phys. Rev. B **5**, 4541 (1972).

[17] G. T. Meaden, Contemp. Phys. **12**, 313 (1971).

[18] M. A. Continentino, S. N. de Medeiros, M. T. D. Orlando, M. B. Fontes, and E. M. Baggio-Saitovitch, Phys. Rev. B **64**, 012404 (2001).